PSFC/JA-10-70

Probing high areal-density (ρR) cryogenic DT implosions using down scattered neutron spectra measured by the Magnetic Recoil Spectrometer (MRS)

J.A. Frenje[1], D.T. Casey[1], C.K. Li[1], F.H. Séguin[1], R.D. Petrasso[1,a)], V. Yu Glebov[2], P.B. Radha[2], T.C. Sangster[2], D.D. Meyerhofer[2,b)], S.P. Hatchett[3], S.W. Haan[3], C.J. Cerjan[3], O.L. Landen[3], K.A. Fletcher[4] and R.J. Leeper[5]

23 April 2010

[1]Massachusetts Institute of Technology, Cambridge, MA 02139 USA
[2]Laboratory for Laser Energetics, University of Rochester, Rochester, New York 14623
[3]Lawrence Livermore National Laboratory, Livermore, California, 94550
[4]Geneseo state University, Geneseo, New York, 14454
[5]Sandia National Laboratory, New Mexico, 87123

[a)] Also Visiting Senior Scientist at the Laboratory for Laser Energetics, University of Rochester.
[b)] Also Department of Mechanical Engineering, and Physics and Astronomy, University of Rochester.

The work described here was supported in part by NLUF (DOE award No. DE-NA0000877), FSC (Rochester Sub award PO No. 415023-G, UR Acct. No. 5-24431), US DOE (Grant No. DE FG03-03SF22691), LLE (No. 412160-001G), and LLNL (No. B504974), and GA under DOE (DE-AC52-06NA27279).

Published in Phys. of Plasmas.

Probing high areal-density (ρR) cryogenic DT implosions using down scattered neutron spectra measured by the Magnetic Recoil Spectrometer (MRS)

J.A. Frenje, D.T. Casey, C.K. Li, F.H. Séguin and R.D. Petrasso[a)]

Plasma Science and Fusion Center, Massachusetts Institute of Technology, Cambridge, Massachusetts, 02139

V. Yu Glebov, P.B. Radha, T.C. Sangster and D.D. Meyerhofer[b)]

Laboratory for Laser Energetics, University of Rochester, Rochester, New York, 14623

S.P. Hatchett, S.W. Haan, C.J. Cerjan and O.L. Landen

Lawrence Livermore National Laboratory, Livermore, California, 94550

K.A. Fletcher

Geneseo state University, Geneseo, New York, 14454

R.J. Leeper

Sandia National Laboratory, New Mexico, 87123

For the first time high-areal density (ρR) cryogenic DT implosions have been probed using down-scattered neutron spectra measured with the Magnetic Recoil Spectrometer (MRS) [J.A. Frenje *et al.*, Rev. Sci. Instrum. **79**, 10E502 (2008)], recently installed and commissioned on OMEGA [T. R. Boehly *et al.*, Opt. Commun. **133**, 495 (1997)]. The ρR data obtained with the MRS have been essential for understanding how assembly of the fuel occurs and for guiding the

cryogenic program at the Laboratory for Laser Energetics (LLE) to ρR values up to ~300 mg/cm^2. ρR data obtained from the well-established Charged Particle Spectrometry (CPS) technique [C.K. Li *et al.*, Phys. of Plasmas **8**, 4902 (2001)] were used to authenticate the MRS data, and the ρR values inferred from these two techniques are similar, indicating that the MRS technique provides high-fidelity ρR data. Recent OMEGA-MRS data and Monte-Carlo simulations have shown that the MRS on the NIF [G.H. Miller *et al.*, E.I. Moses and C.R. Wuest, Nucl. Fusion **44**, S228 (2004)] will meet most of the absolute and relative requirements for determining ρR, ion temperature (T_i) and neutron yield (Y_n) in both low-yield deuterium-lean H-doped THD implosions and high-yield DT implosions.

[a] Also Visiting Senior Scientist at the Laboratory for Laser Energetics, University of Rochester.

[b] Also Dept. of Mechanical Engineering and Physics, and Astronomy, University of Rochester.

I. Introduction

Proper assembly of capsule mass, as manifested through the evolution of fuel areal density (ρR)[1-3], is essential for achieving hot-spot ignition planned at the National Ignition Facility (NIF)[4]. Experimental information about ρR and ρR asymmetries, ion temperature (T_i) and yield (Y_n) are therefore critical for understanding how the assembly of the fuel occurs. To obtain this information, a neutron spectrometer, called a Magnetic Recoil Spectrometer (MRS), is being implemented to measure the absolute neutron spectrum in the range 5 to 30 MeV[5]. This range covers all essential details of the spectrum, allowing the determination of ρR, Y_n, T_i, and possible non-thermal features in the neutron spectrum, as discussed in reference [5]. Another MRS has been built and activated on OMEGA[6] for diagnosing energy-scaled low-adiabat

cryogenic deuterium-tritium (DT) implosions[7]. This allows for experimental validation of the direct-drive ignition-capsule design prior to any experiments at the NIF. As there are currently no other ways to diagnose ρR values larger than ~200 mg/cm^2,[8] the MRS is now playing an important role at OMEGA[9,10]. The MRS will also play a critical role in guiding the National Ignition Campaign (NIC)[11] towards the demonstration of thermonuclear ignition and net energy gain.

This paper is structured as follows: Section II discusses the principle and design of the MRS at OMEGA and the NIF. Section III presents the results from the first measurements of the down-scattered neutron spectrum at OMEGA, from which ρR in plastic-capsule implosions and low-adiabat cryogenic DT implosions have been inferred. Section IV, discusses the *ab initio* (first principle) characterization of the MRS, and its performance of probing high-ρR implosions, at the NIF. Section V summarizes the paper.

II. The Magnetic Recoil Spectrometer (MRS) at OMEGA and the NIF

A. MRS principle

The MRS consists of three main components, as shown in Fig. 1; a CH (or CD) foil positioned 10 and 26 cm to the implosion on OMEGA and the NIF, respectively, for production of recoil protons (or deuterons) from incident neutrons; a focusing magnet, located outside the target chamber on both OMEGA and the NIF, for energy dispersion and focusing of forward-scattered recoil particles onto the focal plane of the spectrometer; and an array of CR-39 detectors, positioned at the focal plane, which records the position of each recoil particle with a detection efficiency of 100%[12]. The spectrum of the recoil protons (or deuterons) is determined by position at the detector plane, and used to infer the absolute neutron spectrum, as discussed in refs. [5,13].

An important strength of the MRS is that the technique can be accurately characterized from first principles (*ab initio*), allowing quantitative signal and background calculations to be performed before the system has been built. An *in situ* calibration is, however, required to check that the system has been built and installed according to specification. As the *ab initio* characterization and *in situ* calibration of the MRS on OMEGA have been described elsewhere[5], these efforts will only be addressed briefly in this paper. An *ab initio* characterization of the MRS on the NIF is on the other hand discussed in detail herein, as the system has undergone significant redesign after reference [5] was published.

B. MRS design considerations

For the MRS to be useful for a large range of applications at OMEGA and the NIF, it has been designed with the highest possible detection efficiency (ε_{MRS}) for a given energy resolution (ΔE_{MRS}), the largest possible single-shot dynamic range, and insensitivity to different types of background. Built-in flexibility has also been included to increase the dynamic range and to more effectively use the MRS for different applications. This is important, as a tradeoff between ε_{MRS} and ΔE_{MRS} must be applied depending on yield. For instance, for practical implementation of low-yield applications, such as measurements of down-scattered neutrons from cryogenic DT implosions at OMEGA and low-yield THD[14] implosions at the NIF, it is necessary to degrade ΔE_{MRS} to increase ε_{MRS}. For high-yield applications, on the other hand, such as measurements of down-scattered neutrons from DT implosions at the NIF, the MRS can be configured to operate in a high-resolution-low-ε_{MRS} mode. Several options are available for configuring the MRS. Either a CH or CD foil can be selected to produce recoil protons or deuterons and thus whether the energy range covered for neutrons is 5.0 – 30 MeV or 3.1 – 16.9 MeV. The foil area and foil

thickness can be adjusted to change the ε_{MRS} and ΔE_{MRS}. Table 1 illustrates the MRS configurations that will be used on the NIF and OMEGA depending on application. The low-resolution-high-efficiency mode (Low-Res) will be used when yields are expected to be below 10^{14} (the values in parentheses are for the MRS at OMEGA when diagnosing cryogenic DT implosions), the medium-resolution-medium-efficiency mode (Med-Res) will be used when yields are expected to be in the range below 10^{14}-10^{18}, (the values in the parentheses are for the MRS at OMEGA when diagnosing plastic-capsule implosions) and the high-resolution-low-efficiency mode (High-Res) can be used when yields are expected to be above ~10^{15}. GEANT4[15] and a Monte-Carlo code were used for the *ab initio* modeling of the MRS, and for assessing its performance of probing high-ρR implosions at the NIF, when operated in the different configurations shown in Table 1. The results from that modeling at 14 MeV are also shown in Table 1.

Table 1: Configurations for the MRS on the NIF and OMEGA. Different configurations will be used depending on application. The OMEGA-MRS settings are shown in the parentheses. The low-resolution-high-efficiency mode (Low-Res) will be used when yields are expected to be below 10^{14} (the values in parentheses are for the MRS at OMEGA when diagnosing cryogenic DT implosions), the medium-resolution-medium-efficiency mode (Med-Res) will be used when yields are expected to be in the range 10^{14}-10^{18} (the values in the parentheses are for the MRS at OMEGA when diagnosing plastic-capsule implosions), and the high-resolution-low-efficiency mode (High-Res) can be used when yields are expected to be above ~10^{15}. The computed ε_{MRS} and ΔE_{MRS} values at 14 MeV are shown as well. Similar performance is obtained with a CD foil that is about a factor of two thinner than the CH foil specified in the table.

	NIF High-Res	NIF (OMEGA) Med-Res	NIF (OMEGA) Low-Res
Yield range	10^{15}-10^{19}	10^{14}-10^{18} (>10^{13})	<10^{14} (>10^{12})
Magnet distance to foil [cm]	570	570 (215)	570 (215)
Magnet aperture area [cm^2]	20	20 (22)	20 (22)
Foil distance to TCC** [cm]	26	26 (10)	26 (10)
Foil area [cm^2]	13	13 (10)	13 (13)
CH-foil thickness [μm]	100	250 (250)	550 (550)
ΔE_{MRS} (FWHM) at 14 MeV [keV]	480	820 (850)	1810 (1830)
ε_{MRS} at 14 MeV	2×10^{-11}	5×10^{-11} (2×10^{-9})	10^{-10} (4×10^{-9})

** *TCC: Target-chamber center*

The principal sources of background are primary neutrons and neutrons scattered by the chamber wall, diagnostics, and other structures surrounding the MRS. Soft and hard X-rays as well as γ-rays are not an issue, since the CR-39 is immune to these types of radiation. Although the CR-39 efficiency for detecting primary neutrons is small[16] ($\varepsilon_{CR\text{-}39} \approx 6\times10^{-5}$), measures are required to reduce the neutron fluence to the required level for successful implementation of the MRS down-scattered neutron measurements at the NIF (and also at OMEGA as discussed in detail in ref [5]). This is achieved by adding polyethylene shielding to the MRS as a first step, and positioning the CR-39 detector array in the shadow of the 50-cm concrete sitting on the 10-cm thick Aluminum target chamber. As the CR-39 detector array is positioned on an off-axis detection plane that is well outside the target chamber, enough space exists to position ~6000 lbs of polyethylene shielding around the MRS (see Figs. 2a-b). Through neutron-transport

simulations using the MCNP code[17], it was established that the shielding reduces the neutron fluence from ~10^{-7} cm^{-2} to ~3×10^{-9} cm^{-2} (E_n > 100 keV) per produced neutron at the CR-39 detector array[18]. Additional reduction of the background (neutron-induced and intrinsic background[19]) is required for successful implementation of the down-scattered neutron measurements for low-yield THD implosions at the NIF (and for cryogenic DT and plastic-capsules implosions at OMEGA). This is accomplished through the use of the Coincidence Counting Technique (CCT)[19] that uses the fact that incident signal particles (protons or deuterons) pass straight through the CR-39 material, resulting in front and backside tracks that are correlated. Signal tracks can therefore be distinguished relatively easily from background tracks (neutron-induced and intrinsic tracks) using the CCT, as the latter tracks are generated mainly on one of the surfaces. Applying the CCT to OMEGA-MRS data demonstrated orders of magnitude *S/B* improvement[19]. For high-yield scenarios, such as an ignited case, the standard counting technique (SCT) has to be applied to the data instead, because the CCT is not effective at high track densities[19]. As a consequence, the S/B ratio is reduced but compensated for a high signal-to-noise (S/N) ratio.

III. Probing plastic and cryogenic-DT implosions at OMEGA using down-scattered neutrons

Diagnosing ρR in DT-filled plastic-capsule implosions has been performed routinely at OMEGA for more than a decade. In these experiments, two magnet based Charged Particle Spectrometers (CPS), shown in Fig. 3, have been used to measure the spectrum of knock-on deuterons (KO-D), elastically scattered by primary DT neutrons, from which fuel ρR can be inferred[20-22]. With the implementation of the MRS (Fig. 3), spectral measurements of the complementary particle, i.e., the down-scattered neutron, are now possible. From the measured

neutron spectrum, the yield ratio between down-scattered neutrons and primary neutrons is determined. This yield ratio, which is called down-scattered fraction (*dsf*), is to the first order proportional to the fuel ρR and probes the compression performance of an implosion[5]. To more accurately establish the relationship between ρR and the measured *dsf*, second-order effects, caused by for instance implosion geometry (profiles of primary source and fuel density), were considered as well. This was done through the use of 1-D Monte-Carlo and hydro modeling of an implosion. Any geometrical 3-D effects have, on the other hand, not been considered in the modeling. This is a topic for future work.

Measurements of the down-scattered neutron spectrum have been conducted for the first time using the MRS on OMEGA. From the measured *dsf* (in the neutron energy range of 10-12 MeV, which corresponds to the deuteron-energy range of about 8-10 MeV), ρR values have been inferred for both low-ρR plastic-capsule implosions and low-adiabat high-ρR cryogenic DT implosions. Data at neutron energies below 10 MeV (or deuteron energies below ~8MeV) was excluded in the analysis as it is comprised primarily by T-T neutrons. ρR data obtained from the well-established CPS technique were used to authenticate the MRS data for the low-ρR plastic-capsule implosions. This authentication is shown in Fig. 4 and Fig. 5 that illustrate integrated MRS and CPS data for a series of eight CH-capsule implosions and a series of five CD-capsule implosions, respectively. As shown by the data, the ρR values inferred from the two different techniques are in good agreement considering the error bars and that ±15% ρR asymmetries are typically observed for these types of implosions. The results indicate that the MRS technique provides high-fidelity ρR data.

An essential step in achieving high fuel compression and high ρR in direct-drive cryogenic DT implosions at OMEGA is to minimize the shock preheating of the main fuel and thus maintain the fuel adiabat at lowest possible value throughout the pulse. This is achieved by

using a multiple-picket laser-drive design[10], in which the individual picket energies and temporal spacing have been tuned to generate a series of decaying shocks that are designed to coalesce simultaneously with the main drive at the inner surface of the main fuel. ρR data obtained with the MRS, CPS1 and CPS2 were used to find the multiple-picket laser-drive design that provides maximum compression. From the shape of the CPS-measured KO-D spectrum the ρR is determined for moderate ρR cryogenic DT implosions (up to ~180 mg/cm^2)[8]. For ρR values higher than ~180 mg/cm^2, the assessment of the implosion performance has to rely on the MRS data. Examples of MRS data obtained for three low-adiabat cryogenic DT implosions are shown in Fig. 6. The MRS-measured deuteron spectra and fits to the measured data, which are convolutions of the neutron spectra and MRS-response function, are shown in Fig. 6a. The modeled neutron spectra that give the best fits to the measured data are shown in Fig. 6b. From the modeled neutron spectra, *dsf* values and thus ρR values were determined for these implosions. A ρR of 83 ± 13 mg/cm^2 was determined for shot 54926 (imploded with an alpha 3 laser pulse), which is ~40% of the 1-D value; a result caused by incorrectly tuned pickets in front of the main drive. A ρR of 179 ± 34 mg/cm^2 was determined for shot 55231 (imploded with an alpha 3 laser pulse). In this case, the multiple pickets were tuned correctly resulting in a ρR value closer to the 1-D value of 220 mg/cm^2. For shot 55723, a ρR of 295 ± 47 mg/cm^2 was determined (imploded with an alpha 2 laser pulse), which is ~95% of the 1-D value. Proper shock timing was applied to this case as well. All ρR data to date inferred from the CPS systems are shown in Fig. 7 as a function of ρR data inferred from the MRS. The open data points were obtained when the imploding capsule was centered close to TCC and had a high-quality ice layer. As expected, these data points are close to the symmetric-implosion line. At ρR values higher than ~180 mg/cm^2 these data points follow the horizontal line at which the CPS technique

has saturated (this upper limit depends somewhat on the density and temperature profiles at bang time). In these high-ρR cases, the assessment of the compression performance has to rely on the MRS data, ice-layer data and offset data. In addition, the solid data points shown in Fig. 7 were obtained when the imploding capsule had a poor ice layer and was significantly offset from TCC. As illustrated by these data points, the poor ice layer and large offset have a detrimental impact on the ρR symmetry of an implosion. This is also generally the case when the offset is larger than the hot-spot radius at peak compression.

IV. *Ab initio* characterization of the MRS at the NIF

The performance of a low-yield THD or a high-yield DT implosion at the NIF can be expressed in terms of the Ignition Threshold Factor (ITF)[23], which is a strong function of the total ρR, T_i and ρR of the hot spot. Although the ITF is not an accurate representation describing the implosion performance, it provides guidance for how accurately these implosion parameters need to be determined at the NIF. From 1-D and 2-D LASNEX[24] simulations it has been concluded that the ITF needs to be determined to an accuracy better than ±30%, which puts strong requirements on the ρR and T_i determination. Table 2 illustrates one set of requirements that is consistent with the ±30% ITF-accuracy requirement for determining *dsf*, T_i and Y_n in THD and DT implosions (in the yield range 10^{14} - 10^{19}). Also shown in the table are the expected absolute and relative measurement uncertainties that the MRS will provide for these implosion parameters. These numbers were determined from MRS spectra simulated by a Monte-Carlo code that used LASNEX simulated neutron spectra as input (see Fig.8). From the MRS signal and background levels, the relative uncertainties were computed, as discussed in Appendix A. The systematic uncertainties are also derived in Appendix A. As shown by the numbers in Table

2, it is clear that the MRS will meet the requirements for diagnosing both low-yield THD and high-yield DT implosions.

Table 2: Requirements and expected uncertainties for the MRS measuring the down-scattered fraction (dsf) (which to the first order depends on ρR), T_i and Y_n produced in THD and DT implosions at the NIF.

		Physics requirements		Expected measurements uncertainties**	
Campaign	Parameter	Absolute	Relative	Absolute (Fig. A1; Table A1)	Relative (Fig. A1)
THD (2×10^{14})	*dsf*	± 7 %	± 5 %	± 6 %	± 4 %
	T_i	± 3 %	± 3 %	± 15 %	± 15 %
	Y_n	± 8 %	± 2 %	± 5 %	± 2 %
THD (10^{16})	*dsf*	± 7 %	± 5 %	± 3 %	± 0.5 %
	T_i	± 3 %	± 3 %	± 3 %	± 1 %
	Y_n	± 8 %	± 2 %	± 4 %	± 0.2 %
DT (10^{17}-10^{19})	*dsf*	*± 7 %*	*± 5 %*	*± 3 %*	*± 0.2 %*
	T_i	*± 3 %*	*± 3 %*	*± 2 %*	*± 0.3 %*
	Y_n	*± 8 %*	*± 2 %*	*± 4 %*	*± 0.1 %*

** *The absolute measurement uncertainties are due to both systematic and statistical uncertainties. The relative uncertainties are only due to statistical uncertainties.*

To accurately determine *dsf* values from measured MRS spectra, different proton-energy, or deuteron-energy, ranges must be used depending on MRS configuration and type of implosion diagnosed. Table 3 illustrates the proton-energy ranges used for the MRS configured with a CH

foil and operated in High-Res, Med-Res and Low-Res mode. These energy ranges were also used to determine the statistical uncertainties for the *dsf* values shown in Table 2.

Table 3: Proton-energy ranges for determining the dsf value from the measured MRS spectra. In the THD case the T-T neutron spectrum sets a lower limit for the dsf determination. The primary peak, broadened by the MRS-response function, sets an upper limit for both the THD and DT case.

	High-Res*	Med-Res*	Low-Res
THD	9.5 – 13.0 MeV	9.4-12.5 MeV	9.3-11.3 MeV
DT	5.0 – 13.0 MeV	5.0-12.5 MeV	5.0-11.3 MeV

* *The useful proton-energy range for the dsf determination is narrower if the implosion ignites. In this case, the upper limit is ~11.5 MeV, as indicated in Fig. 8c.*

V. Summary

For the first time measurements of down-scattered neutron spectra have been conducted using the MRS, recently installed and commissioned on OMEGA. From the measured down-scattered neutron spectrum, a *dsf* value has been measured from which ρR has been inferred for both low-ρR plastic-capsule implosions and low-adiabat high-ρR cryogenic DT implosions. ρR data obtained from the well-established CPS technique were used to authenticate the MRS data for these low-ρR plastic-capsule implosions, and results illustrate a good agreement between the two techniques. In addition, the ρR data obtained from the MRS for the low-adiabat high-ρR cryogenic DT implosions have been essential for understanding how assembly of the fuel occurs and for guiding the cryogenic program at LLE to ρR values up to ~300 mg/cm^2.

Recent OMEGA-MRS data and Monte-Carlo simulations indicate that the MRS on the NIF will meet most of the absolute and relative requirements for determining ρR, T_i and Y_n in both low-yield THD and high-yield DT implosions. The work described here was supported in part by US DOE (Grant No. DE-FG03-03SF22691), LLE (No.412160-001G), LLNL (No.B504974), and GA under DOE (DE-AC52-06NA27279).

Appendix A: Statistical and systematic uncertainties for the MRS at the NIF

From the simulated MRS signal and background spectra (three example spectra are shown in Fig. 8) it is readily straight forward to calculate the statistical uncertainties for the measured *dsf*, T_i and Y_n. Equation (A1) represents the statistical uncertainty associated with the *dsf* value; equation (A2) represents the statistical uncertainty associated with T_i; and equation (A3) represents the statistical uncertainty associated with Y_n,

$$\frac{\Delta(dsf)}{dsf} = \frac{\sqrt{S_{ds} + 2B}}{S_{ds}}, \tag{A1}$$

$$\frac{\Delta T_i}{T_i} = \left[1 + \left(\frac{\Delta E_{MRS}}{\Delta E_D}\right)^2\right] \frac{1}{\sqrt{S_p}}, \tag{A2}$$

[25]

$$\frac{\Delta Y_n}{Y_n} = \frac{1}{\sqrt{S_p}}. \tag{A3}$$

Here, S_{ds} is the integrated down-scattered neutron signal in the selected energy range shown in Table 3, B is the total background in this energy range, ΔE_D is the width of the Doppler broadened neutron spectrum, which is to the first order equal to $177\sqrt{T_i}$ for the DT reaction (T_i given in keV),[26] and S_p is the integrated primary neutron signal. As shown by equation (A3), the

yield uncertainty can be expressed in terms of only S_p because the primary signal is orders of magnitude higher than the background. These equations were applied to MRS spectra for thirteen different implosions, which resulted in the statistical uncertainties shown in Fig. A1.

For illustration purposes, as well as for calculating systematical uncertainties involved with the MRS, it is useful to express ε_{MRS} and ΔE_{MRS} as[5]

$$\varepsilon_{MRS}(E_n) = \frac{\Omega_n}{4\pi} \cdot n_i \cdot t_f \int^{"\Omega_r"} \frac{d\sigma(E_n)}{d\Omega_{lab}} d\Omega, \tag{A4}$$

and

$$\Delta E_{MRS}(E_n) \approx \sqrt{\Delta E_f^2(E_n) + \Delta E_k^2(E_n) + \Delta E_m^2(E_n)}, \tag{A5}$$

respectively. Here, Ω_n is the solid angle subtended by the foil, n_i is the hydrogen (or deuterium) number density in the foil, t_f is the thickness of the foil, and $d\sigma(E_n)/d\Omega_{lab}$ is the differential elastic-cross section in the laboratory frame, "Ω_r" is the solid angle subtended by the aperture in front of the magnet, ΔE_f is the energy broadening in the conversion foil, ΔE_k is the kinematic energy broadening, and ΔE_s is the ion-optical broadening. As the solid angle subtended by the foil can be expressed in terms of foil area (A_f) and foil distance (R_f), and the differential elastic-cross section integrated over the solid angle subtended by the magnet aperture can be approximated by $d\sigma/d\Omega_{lab}(E_n,0°) \cdot [A_a/R_a^2]$ (where A_a is the magnet aperture area and R_a is the magnet-aperture distance to the foil), equation (A4) can be rewritten as

$$\varepsilon_{MRS}(E_n) \approx \frac{A_f}{4\pi R_f^2} \cdot n_i \cdot t_f \cdot \frac{d\sigma(E_n,0°)}{d\Omega_{lab}} \cdot \frac{A_a}{R_a^2}. \tag{A6}$$

Using equation (A6), Y_n and the *dsf* value can now be expressed as

$$Y_n \approx \frac{S_p}{\frac{A_f}{4\pi R_f^2} \cdot n_i \cdot t_f \cdot \frac{d\sigma(E_n,0°)}{d\Omega_{lab}} \cdot \frac{A_a}{R_a^2}} \tag{A7}$$

and

$$dsf \approx \frac{\frac{d\sigma(p,0°)}{d\Omega_{lab}}}{\frac{d\sigma(ds,0°)}{d\Omega_{lab}}} \frac{S_{ds}}{S_p}, \tag{A8}$$

respectively. Here, *p* and *ds* in equation (A8) represents the average energy of primary and down-scattered neutrons, respectively. An expression for the systematic uncertainty involved with the *dsf* and Y_n measurements can now be derived from equations (A7) and (A8), i.e.,

$$\frac{\sigma_{Y_n}}{Y_n} \approx \sqrt{\left(\frac{\sigma_{A_f}}{A_f}\right)^2 + 4\left(\frac{\sigma_{R_f}}{R_f}\right)^2 + \left(\frac{\sigma_{n_i}}{n_i}\right)^2 + \left(\frac{\sigma_{t_f}}{t_f}\right)^2 + \left(\frac{\sigma_{\sigma(0°)}}{\sigma(0°)}\right)^2 + \left(\frac{\sigma_{A_a}}{A_a}\right)^2 + 4\left(\frac{\sigma_{R_a}}{R_a}\right)^2} \tag{A9}$$

and

$$\frac{\sigma_{dsf}}{dsf} \approx \sqrt{\left(\frac{\sigma_{\frac{d\sigma(p,0°)}{d\Omega_{lab}}}}{\frac{d\sigma(p,0°)}{d\Omega_{lab}}}\right)^2 + \left(\frac{\sigma_{\frac{d\sigma(ds,0°)}{d\Omega_{lab}}}}{\frac{d\sigma(ds,0°)}{d\Omega_{lab}}}\right)^2}, \tag{A10}$$

respectively. As shown by equation (A10), the systematic uncertainty for the *dsf* value depends only on the uncertainties in the differential elastic-cross sections at the different energies. This is an important feature of the MRS that can be explained by the fact that the systematic uncertainties associated with the MRS geometry are cancelled out, i.e., simultaneous measurements of the down-scattered and primary neutrons are exposed to identical geometry-related uncertainties. Table A1 illustrates the actual systematic uncertainties for the different parameters expressed in equations (A9) and (A10), and their combined contribution to the total error for the different MRS configurations shown in Table 2.

Table A1: Systematic uncertainties for the different parameters expressed in equations (A9) and (A10), and their combined contribution to the total error for the different MRS configurations shown in Table 2. These numbers are only valid for the CH foils. The cross–section uncertainties involved with the CD foil are about a factor of 2 higher than the ones involved with the CH foil.

	Absolute	High-Res [%]	Med-Res [%]	Low-Res [%]
Foil area uncertainty	±0.3 cm^2	±2.3	±2.3	±2.3
Foil distance uncertainty	±0.1 cm	±0.4	±0.4	±0.4
Number density uncertainty	±10^{21} cm^3	±1.3	±1.3	±1.3
Foil thickness uncertainty	±2.0 μm	±2.0	±0.8	±0.4
Cross section uncertainty (*p*)	±0.01 b	±1.4	±1.4	±1.4
Cross section uncertainty (*ds*)	±0.03 b	±2.5	±2.5	±2.5
Magnet aperture area uncertainty	±0.2 cm^2	±1.0	±1.0	±1.0
Magnet aperture distance uncertainty	±0.1 cm	±0.02	±0.02	±0.02
Total uncertainty for Y_n		±4.5	±4.1	±4.0
Total uncertainty for *dsf*		±2.9	±2.9	±2.9

References

1. S.W. Haan, S. Pollaine, J.D. Lindl, L.J. Suter, R.L. Berger, L.V. Powers, W.E. Alley, P.A. Amendt, J.A. Futterman, W.K. Levedahl, M.D. Rosen, D.P. Rowley, R.A. Sacks, A.I. Shestakov, G.L. Strobel, M. Tabak, S.V. Weber and G.B. Zimmerman, Phys. Plasmas **2**, 2480 (1995).
2. J.D. Lindl, R.L. McCrory and E.M. Campbell, Phys. Today **45**, 32 (1992).
3. M.D. Rosen, Phys. Plasmas **3**, 1803 (1996).
4. G.H. Miller, E.I. Moses and C.R. Wuest, Nucl. Fusion **44**, S228 (2004).
5. J.A. Frenje, D.T. Casey, C.K. Li J.R. Rygg, F.H. Séguin, and R.D. Petrasso, V.Yu Glebov, D.D. Meyerhofer, T.C. Sangster, S. Hatchett, S. Haan, C. Cerjan, O. Landen, M. Moran, P. Song, D.C. Wilson and R.J. Leeper, Rev. Sci. Instrum. **79**, 10E502 (2008).
6. T.R. Boehly, D.L. Brown, R.S. Craxton, R.L. Keck, J.P. Knauer, J.H. Kelly, T.J. Kessler, S.A. Kumpan, S.J. Bucks, S.A. Letzring, F.J. Marshall, R.L. McCrory, S.F.B. Morse, W. Seka, J.M. Soures and C.P. Verdon, Opt. Commun. **133**, 495 (1997).
7. R.L. McCrory, D.D. Meyerhofer, R. Betti, R.S. Craxton, J.A. Delettrez, D.H. Edgell, V.Yu. Glebov, V.N. Goncharov, D.R. Harding, D.W. Jacobs-Perkins, J.P. Knauer, F.J. Marshall, P.W. McKenty, P.B. Radha, S.P. Regan, T.C. Sangster, W. Seka, R.W. Short, S. Skupsky, V.A. Smalyuk, J.M. Soures, C. Stoeckl, B. Yaakobi, D. Shvarts, J.A. Frenje, C.K. Li, R.D. Petrasso and F.H. Séguin, Phys. Plasmas 15, 055503 (2008).
8. J.A. Frenje, C.K. Li, F.H. Séguin, D.T. Casey, R.D. Petrasso, T.C. Sangster, R. Betti, V.Yu. Glebov and D.D. Meyerhofer, Phys. Plasmas **16**, 042704 (2009).
9. T.C. Sangster V.N. Goncharov, R. Betti, T.R Boehly, D.T. Casey, T.J.B. Collins, R.S. Craxton, J.A. Delettrez, D.H. Edgell, R. Epstein, K.A. Fletcher, J.A. Frenje, Y.Yu. Glebov, D.R. Harding, S.X. Hu, I.V. Igumenschev, J.P. Knauer, S.J. Loucks, C.K. Li, J.A. Marozas,

F.J. Marshall, R.L. McCrory, P.W. McKenty, D.D. Meyerhofer, P.M. Nilson, S.P. Padalino, R.D. Petrasso, P.B. Radha, S.P. Regan, F.H. Seguin, W. Seka, R.W. Short, D. Shvarts, S. Skupsky, V.A. Smalyuk, J.M. Soures, C. Stoeckl, W. Theobald and B. Yaakobi, "Shock-Tuned Cryogenic DT Implosion Performance on OMEGA", submitted to Phys. Plasmas (2009).

10. V.N Goncharov, T.C. Sangster, S. Hu, I. Igumenshchev, R.L. McCrory. D.D. Meyerhofer, P.B. Radha, S. Skupsky, D.T. Casey, J.A. Frenje and R.D Petrasso, "Multiple-picket cryogenic designs for OMEGA and the NIF", submitted to Phys. Rev. Letter (2009).
11. E.I. Moses, AIP Conf. Proc. 1154, 53 (2009).
12. F.H. Séguin, J.A. Frenje, C.K. Li, D.G. Hicks, S. Kurebayashi, J.R. Rygg, B.-E. Schwartz, and R.D. Petrasso, S. Roberts, J.M. Soures, D.D. Meyerhofer, T.C. Sangster, J.P. Knauer, C. Sorce, V.Yu. Glebov, C. Stoeckl, T.W. Phillips , R.J. Leeper, K. Fletcher and S. Padalino, Rev. Sci. Instrum. **74**, 975 (2003).
13. J.A. Frenje, K.M. Green, D.G. Hicks, C.K. Li, F.H. Séguin, R.D. Petrasso, T.C. Sangster, T.W. Phillips, V.Yu. Glebov, D.D. Meyerhofer, S. Roberts, J.M. Soures and C. Stoeckl, Rev. Sci. Instrum. **72**, 854 (2001).
14. A THD capsule is filled with more deuterium-lean fuel mixtures and H-dopant levels up to 25% (by atom).
15. S. Agostinelli, J. Allison, K. Amako, J. Apostolakis, H. Araujo, P. Arce, M. Asai, D. Axen, S. Banerjee, G. Barrand, F. Behner, L. Bellagamba, J. Boudreau, L. Broglia, A. Brunengo, H. Burkhardt, S. Chauvie, J. Chuma, R. Chytracek, G. Cooperman, *et al.,* Nucl. Instr. and Methods, A311, 595 (1992).

16. J.A. Frenje, C.K. Li, F.H. Séguin, S. Kurebayashi, R.D. Petrasso, J.M. Soures, J. Delettrez, V.Yu. Glebov, D.D. Meyerhofer, P.B. Radha, S. Roberts, T.C. Sangster, S. Skupsky and C. Stoeckl, Phys. Plasmas **9**, 4719 (2002).
17. X-5 Monte Carlo Team. MCNP-A general Monte Carlo n-particle transport code. LA-UR-03-1987, Version 5, Los Alamos National Laboratory (2003).
18. D.T Casey, J.A. Frenje, C.K. Li, F.H. Séguin, R.D. Petrasso, V.Yu. Glebov, D.D. Meyerhofer and T.C. Sangster, "Minimizing neutron background for the Magnetic Recoil Spectrometer at OMEGA and the NIF", to be submitted to Rev. Sci. Instrum. (2010).
19. D.T Casey, J.A. Frenje, C.K. Li, F.H. Séguin, R.D. Petrasso, V.Yu. Glebov, D.D. Meyerhofer and T.C. Sangster, "The Coincidence Counting Technique for enhanced background rejection in the MRS data", to be submitted to Rev. Sci. Instrum. (2010).
20. C.K. Li, F.H. Séguin, D.G. Hicks, J.A. Frenje, K.M. Green, S. Kurebayashi, R.D. Petrasso, D.D. Meyerhofer, J. M. Soures, V. Yu. Glebov, R. L. Keck, P.B. Radha, S. Roberts, W. Seka, S. Skupsky, C. Stoeckl and T.C. Sangster, Phys. of Plasmas **8**, 4902 (2001).
21. S. Skupsky, R.W. Short, T. Kessler, R.S. Craxton, S. Letzring, and J.M. Soures, J. Appl. Phys. **66**, 3456 (1989).
22. S. Kacenjar, S. Skupsky, A. Entenberg L. Goldman and M. Richardson, Phys. Rev. Lett. **49**, 463 (1982).
23. B.K. Spears, S. Brandon, D. Clark, C. Cerjan, J.Edwards, O. Landen, J. Lindl, S. Haan, S. Hatchett, J. Salmonson, P. Springer, S.V. Weber and D. Wilson, "Prediction of ignition implosion performance using measurements of low-deuterium surrogates", to be submitted to Phys. Plasmas (2010).
24. G. Zimmerman and W. Kruer, Comments Plasma Phys. Control. Fusion **11**, 51 (1975).

25. O.N. Jarvis, G. Gorini, M. Hone, J. Källne, G. Sadler, V. Merlo and P. van Belle, Rev. Sci. Instrum. **57**, 1717 (1986).

26. H. Brysk, Plasma Phys. **15**, 611 (1973).

Figure 1 (Color online): A schematic drawing of the MRS, including the CH (or CD) foil, magnet, and CR-39 detector array. The foil is positioned 10 cm and 26 cm from the implosion at OMEGA and the NIF, respectively; the magnet is positioned outside the target chamber on both facilities, i.e., 215 cm to the foil on OMEGA and 570 cm to the foil on the NIF. Important to the overall design is that the same magnet design is used in both the OMEGA-MRS and NIF-MRS. For detection of the forward scattered recoil protons (or deuterons) when using a CH foil (or CD foil), eleven and nine 6×5 cm^2 CR-39 detectors are positioned at the focal plane in the OMEGA-MRS and NIF-MRS, respectively. The trajectories shown are for proton energies from 5 to 30 MeV, corresponding to deuteron energies from 2.5 to 15 MeV. The length of the detector plane is 166 cm and 84 cm for the OMEGA-MRS and NIF-MRS, respectively.

Figure 2 (Color online): (a) An engineering drawing of the MRS positioned onto the NIF-target chamber at the line-of-sight 77°-324°. For maximum suppression of the neutron-induced background the CR-39 detector array is positioned in the shadow of the 50-cm concrete (marked blue) sitting on the 10-cm thick Aluminum target chamber and fully enclosed by ~6000 lbs of polyethylene shielding (marked grey and green). (b) A vertical cross cut through the MRS illustrating the various components in the system, i.e., the magnet, CR-39 detector array, alignment system and shielding. The Diagnostic Insertion Manipulator (DIM) 90°-315°, not shown in these figures, is planned to be used for the insertion of the foil to a distance of 26 cm from the implosion.

Figure 3 (Color online): MRS, CPS1 and CPS2 on the OMEGA chamber. The MRS is shown here without the 2000 lbs shielding that surrounds the diagnostic. The line of sight for each

diagnostic is illustrated in terms of the polar angle ϕ and azimuthal angle θ. These spectrometers are used to measure the spectra of KO-D's (CPS1 and CPS2) and down-scattered neutrons (MRS), from which fuel ρR and ρR asymmetries in cryogenic DT implosions are inferred.

Figure 4 (Color online): Integrated MRS and CPS data obtained for a series of eight CH-capsule implosions producing 1.6×10^{14} primary neutrons (neutron-averaged T_i is 5.3 keV). In each shot, a capsule with a 15-μm thick CH shell filled with 15-atm DT gas was imploded with a 1-ns square pulse delivering ~23 kJ of laser energy. (a) The MRS-measured deuteron spectrum and fit to the measured spectrum, which are convolutions of the underlying neutron spectrum and MRS-response function. In these measurements, the MRS was operated with a CD foil in Med-Res mode (see Table 1). From the *dsf* value determined from the modeled neutron spectrum, shown in (b), a total ρR (fuel+shell) of 65 ± 9 mg/cm^2 was inferred. Data at neutron energies below 10 MeV was excluded in the analysis as it is comprised primarily by T-T neutrons. (c) CPS2 data illustrating a spectrum of KO-D's produced in the fuel. From the yield in the high-energy peak[20] (marked grey) a fuel ρR of 9 ± 2 mg/cm^2 was inferred. (d) CPS1 data illustrating a spectrum of knock-on protons (KO-P) produced in the shell. From the yield in the plateau[20] (marked grey) a shell ρR of 47 ± 9 mg/cm^2 was inferred. A total ρR of 56 ± 10 mg/cm^2 is thus determined from the CPS1 and CPS2 data. Given that ±15% ρR asymmetries are typically observed for this type of implosion, the ρR values determined from the MRS and CPS data are in good agreement.

Figure 5 (Color online): Integrated MRS and CPS data obtained for a series of five CD-capsule implosions producing 2.6×10^{14} primary neutrons (neutron-averaged T_i is 8.0 keV). In each shot, a capsule with a 10-μm thick CD shell filled with 10-atm DT gas was imploded with a 1-ns

square pulse delivering ~23 kJ of laser energy. (a) The MRS-measured deuteron spectrum and fit to the measured spectrum, which are convolutions of the underlying neutron spectrum and MRS-response function. In these measurements, the MRS was operated with a CD foil in Med-Res mode (see Table 1). From the *dsf* value determined from the modeled neutron spectrum, shown in (b), a total ρR (fuel+shell) of 44 ± 8 mg/cm^2 was inferred. Data at neutron energies below 10 MeV was excluded in the analysis as it is primarily comprised by T-T neutrons. (c) CPS2 data illustrating a spectrum of KO-D's produced in the fuel and shell. From the yield in the high-energy peak[20] (marked grey) a total ρR of 40 ± 6 mg/cm^2 was inferred, which is in excellent agreement with the ρR value determined from the MRS.

Figure 6 (Color online): MRS data obtained for three low-adiabat cryogenic DT implosions producing neutron yields in the range 2×10^{12} to 4×10^{12} (neutron-averaged T_i is ~2 keV for these implosions). (a) MRS-measured deuteron spectra for the three implosions and fits to the measured spectra, which are convolutions of the underlying neutron spectra and the MRS-response function. In these measurements, the MRS was operated with a CD foil in Low-Res mode (see Table 1). From the modeled neutron spectra, shown in (b), *dsf* values and thus ρRs were determined for the three implosions. A ρR of 83 ± 13 mg/cm^2 was determined for shot 54926 (imploded with an alpha 3 laser pulse), which is just ~40% of the 1-D value; a result of a poorly designed laser drive. A ρR of 179 ± 34 mg/cm^2 was determined for shot 55231 (imploded with an alpha 3 laser pulse). In this case the picket pulses in front of the main laser drive were tuned correctly resulting in a ρR value closer to the 1-D value of 220 mg/cm^2. For shot 55723, a ρR of 295 ± 47 mg/cm^2 was determined (imploded with an alpha 2 laser pulse), which is in

agreement with the 1-D ρR value considering the error bar. An optimal multiple-picket laser drive was applied in this case as well.

Figure 7 (Color online): ρR inferred from CPS data as a function of ρR inferred from MRS data. The open data points were obtained when the imploding capsule had a high-quality ice layer and centered close to target-chamber center (TCC), while the solid points were obtained when the imploding capsule had a poor ice layer and significantly offset from TCC. As expected, the open data points are close to the symmetric-implosion line. At ρR values higher than ~180 mg/cm^2 the assessment of the compression performance has to rely on the MRS data, ice-layer data and offset data, as the CPS technique has saturated. As shown by the solid data points, the poor ice layer and large offset have a detrimental impact on the ρR symmetry of an implosion. This is also generally the case when the offset is larger than the hot-spot radius at peak compression

Figure 8 (Color online): A set of three LASNEX simulated neutron spectra and associated MRS signal and background spectra for three different NIF implosions; (a) a low-yield deuterium-lean THD implosion (the dashed line indicates the T-T neutron spectrum, (b) a fizzle DT implosion, and (c) an ignited DT implosion. The T-T neutron component in the two DT cases is insignificant and thus not shown. The total ρR and Y_n for each implosion are shown in each figure. These spectra were simulated for the MRS configured in Med-Res mode with a CH foil. The CCT, recently developed and now routinely used to analyze OMEGA-MRS data, was applied to determine the MRS signal and background spectra for the low-yield THD and fizzle DT implosions. For the ignited case, standard counting technique (SCT) was applied to the data as the CCT is not effective at high track densities[19]. As shown by the spectra, excellent S/B is achieved for the *dsf*, T_i and Y_n measurements.

Figure A1 (Color online): Statistical measurement uncertainty for *dsf* (a), T_i (b), and Y_n (c) as a function of neutron yield. Thirteen simulated neutron spectra and MRS signal and background spectra were used in these calculations. The relative requirements, illustrated in Table 2, are indicated by the dashed lines.

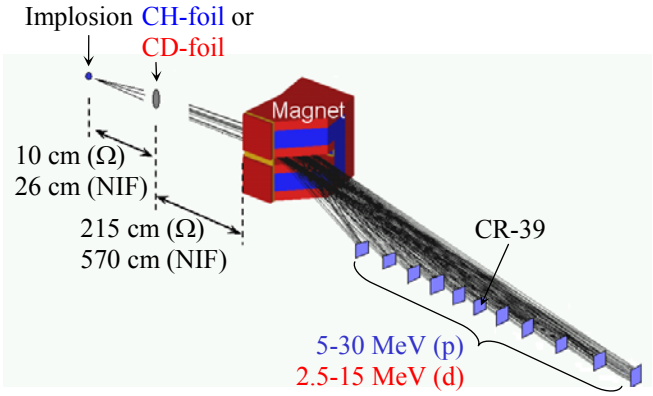
Implosion CH-foil or
CD-foil
Magnet
10 cm (Ω)
26 cm (NIF)
215 cm (Ω)
570 cm (NIF)
CR-39
5-30 MeV (p)
2.5-15 MeV (d)

Figure 1

(a)

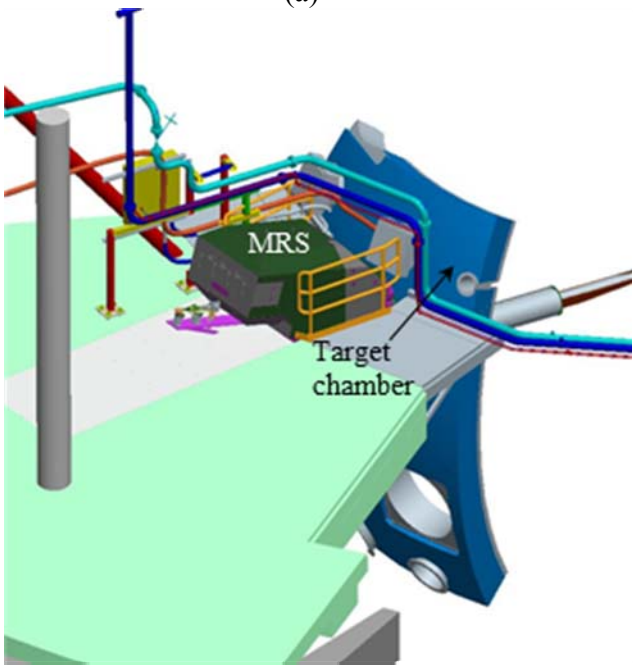
MRS
Target
chamber

(b)

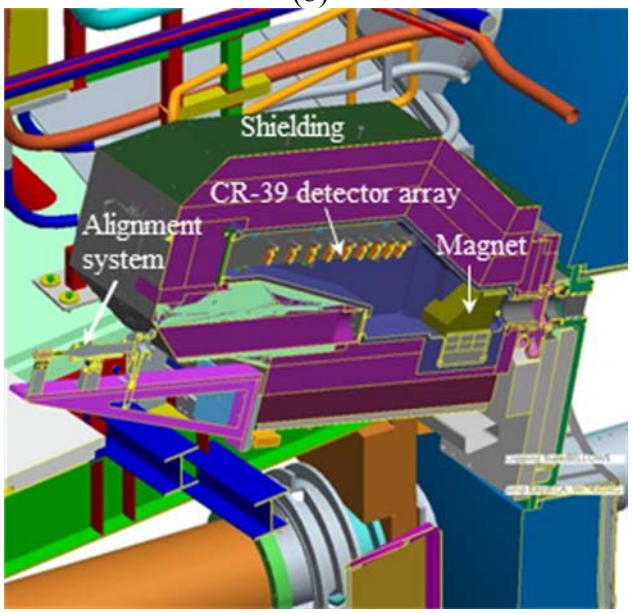
Shielding
CR-39 detector array
Alignment
system
Magnet

Figure 2

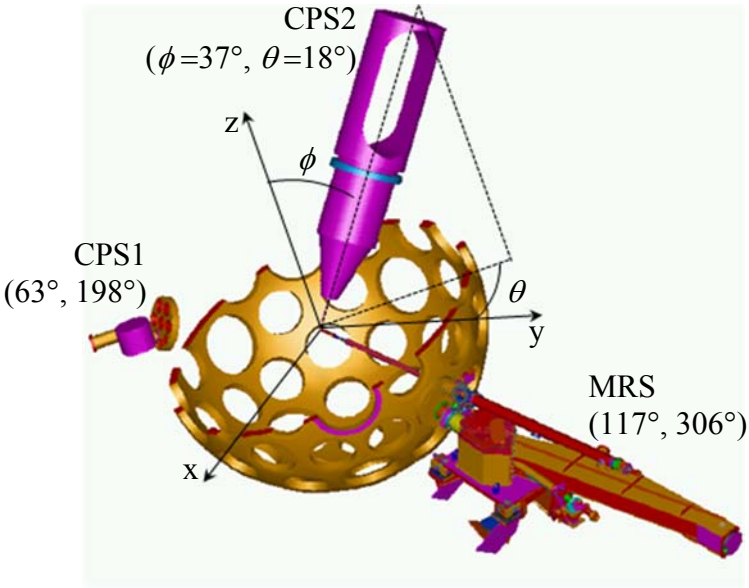

Figure 3

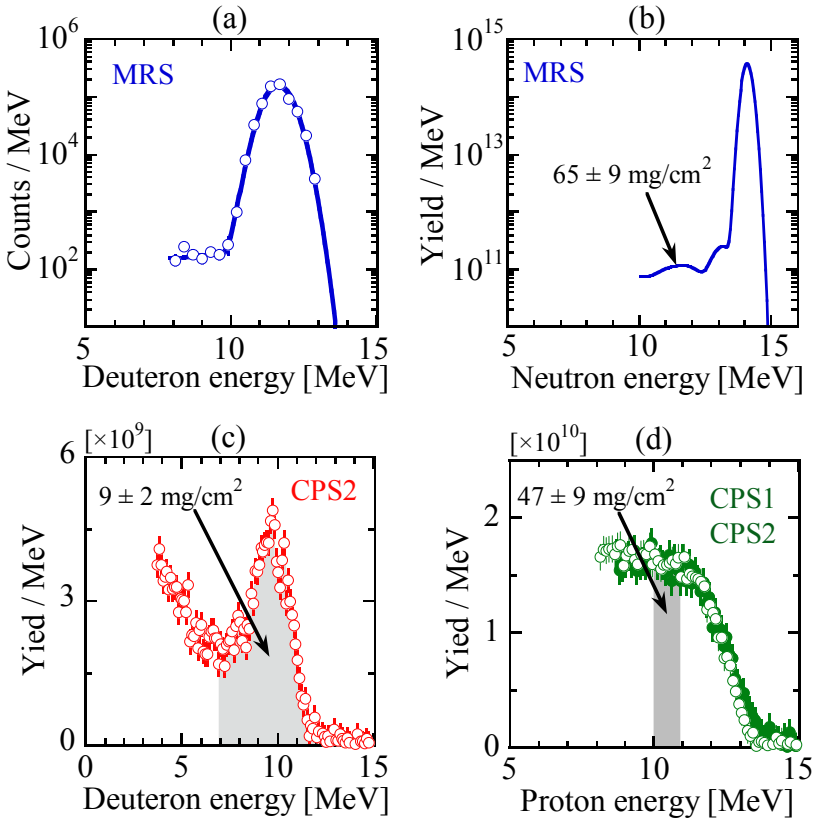
(a)
MRS
Counts / MeV
Deuteron energy [MeV]
(b)
MRS
65 ± 9 mg/cm2
Yield / MeV
Neutron energy [MeV]
[×10^9]
(c)
9 ± 2 mg/cm2
CPS2
Yied / MeV
Deuteron energy [MeV]
[×10^10]
(d)
47 ± 9 mg/cm2
CPS1
CPS2
Yied / MeV
Proton energy [MeV]

Figure 4

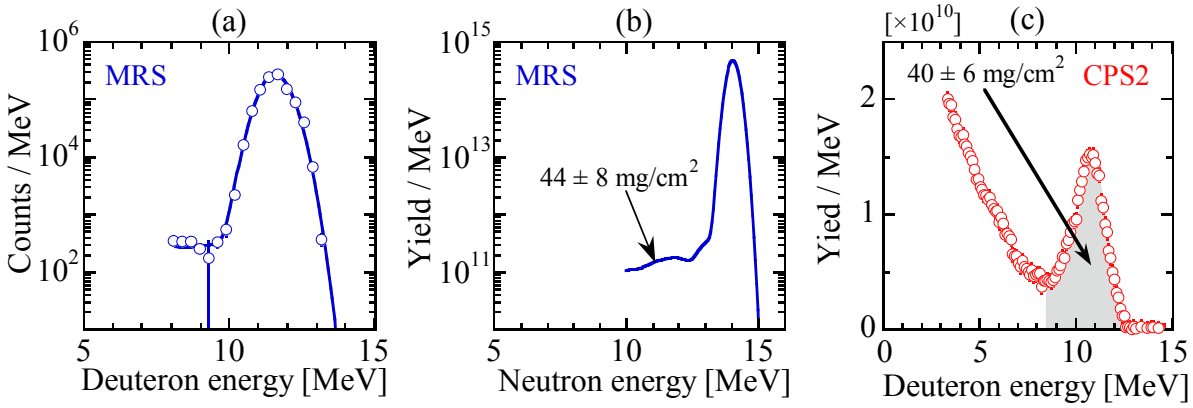
(a)
MRS
Counts / MeV
Deuteron energy [MeV]
(b)
MRS
44 ± 8 mg/cm2
Yield / MeV
Neutron energy [MeV]
[×10^10]
(c)
40 ± 6 mg/cm2
CPS2
Yied / MeV
Deuteron energy [MeV]

Figure 5

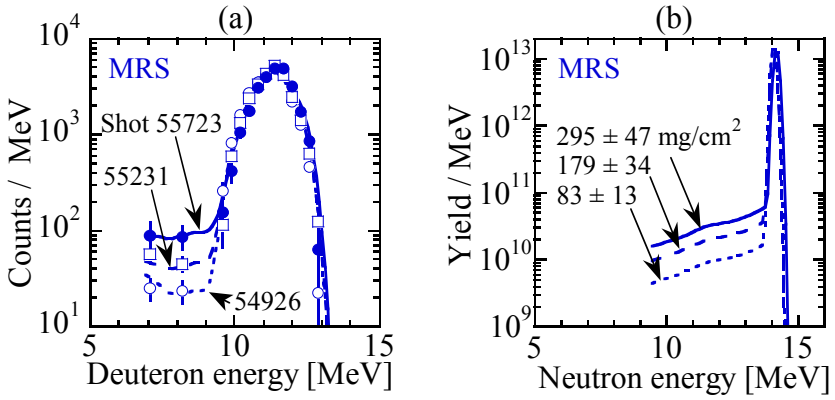
(a)
MRS
Shot 55723
55231
54926
Counts / MeV
Deuteron energy [MeV]
(b)
MRS
295 ± 47 mg/cm2
179 ± 34
83 ± 13
Yield / MeV
Neutron energy [MeV]

Figure 6

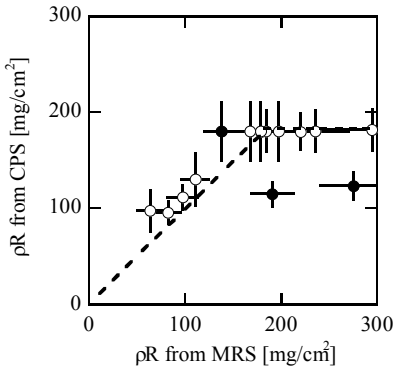

Figure 7

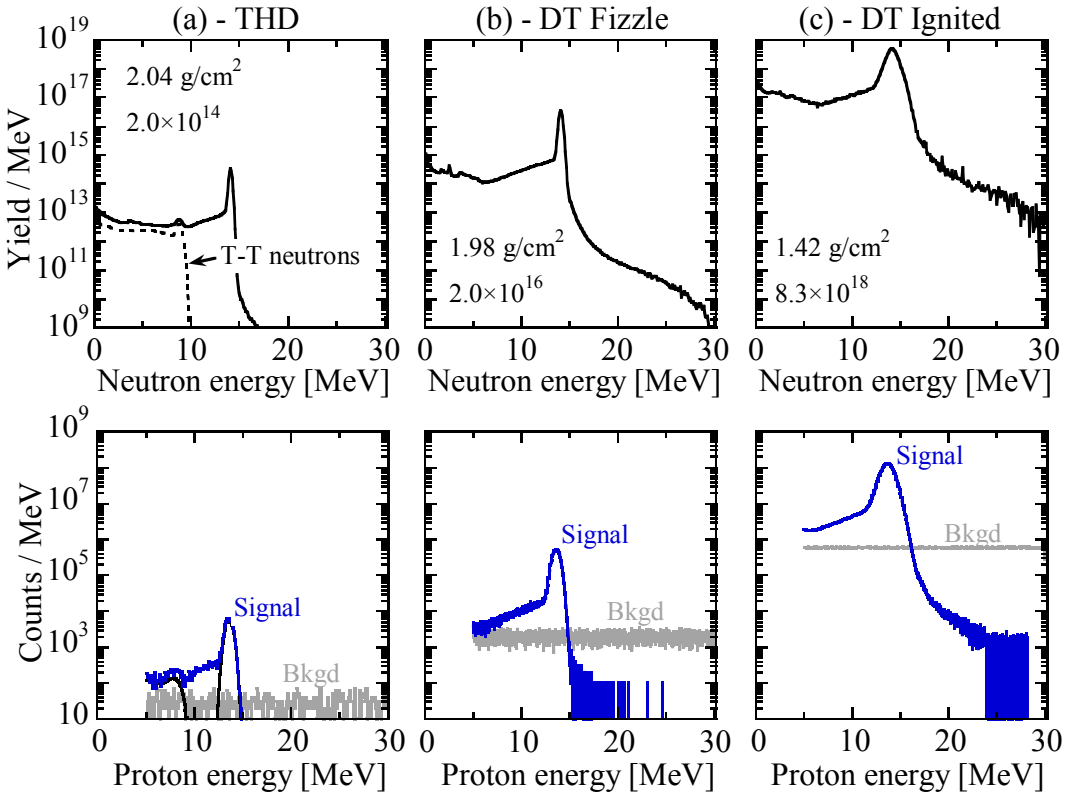
(a) - THD
(b) - DT Fizzle
(c) - DT Ignited
Yield / MeV
2.04 g/cm2
2.0×1014
T-T neutrons
1.98 g/cm2
2.0×1016
1.42 g/cm2
8.3×1018
Neutron energy [MeV]
Counts / MeV
Signal
Bkgd
Proton energy [MeV]

Figure 8

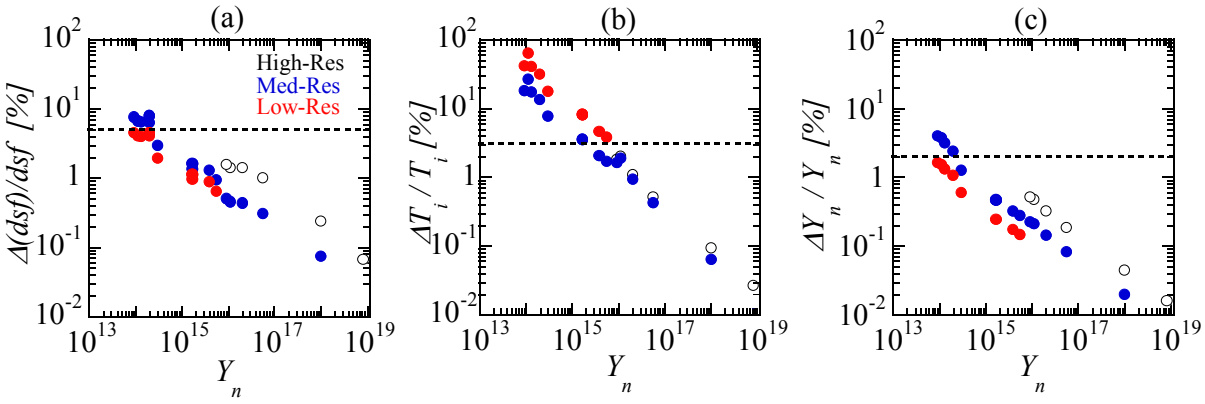
(a)
(b)
(c)
High-Res
Med-Res
Low-Res
$\Delta(dsf)/dsf$ [%]
$\Delta T_i / T_i$ [%]
$\Delta Y_n / Y_n$ [%]
Y_n
10^{2}
10^{1}
1
10^{-1}
10^{-2}
10^{13}
10^{15}
10^{17}
10^{19}

Figure 9